

1 Data acquisition electronics and reconstruction software
 2 for directional detection of Dark Matter with MIMAC

3 O. Bourrion^{a,*}, G. Bosson^a, C. Grignon^a, J. L. Bouly^a, J. P. Richer^a, O.
 4 Guillaudin^a, F. Mayet^a, D. Santos^a

5 ^a*Laboratoire de Physique Subatomique et de Cosmologie,*
 6 *Université Joseph Fourier Grenoble 1,*
 7 *CNRS/IN2P3, Institut Polytechnique de Grenoble,*
 8 *53, rue des Martyrs, Grenoble, France*

9 **Abstract**

10 Directional detection of galactic Dark Matter requires 3D reconstruction of low
 11 energy nuclear recoils tracks. A dedicated acquisition electronics with auto trig-
 12 gering feature and a real time track reconstruction software have been developed
 13 within the framework of the MIMAC project of detector. This auto-triggered
 14 acquisition electronic uses embedded processing to reduce data transfer to its
 15 useful part only, i.e. decoded coordinates of hit tracks and corresponding energy
 16 measurements. An acquisition software with on-line monitoring and 3D track
 17 reconstruction is also presented.

18 **1. Introduction**

19 Directional detection is a promising search strategy of galactic Dark Matter.
 20 The idea is to take advantage on the rotation of the Solar system around the
 21 galactic center to show a direction dependance of WIMP signals, which should
 22 then be clearly discriminated from background ones [1, 2, 3, 4, 5]. Recently, a
 23 statistical map-based analysis has been developed [6], showing for the first time
 24 the possibility to extract from data samples of forthcoming directional detec-
 25 tors, both the main direction of the incoming events, thus proving the galactic
 26 origin of the signal, and the number of WIMP events contained in the map.
 27 Several directional detectors are being developed and/or operated : MIMAC [7],
 28 DRIFT [8], NEWAGE [9], DM-TPC [10]. A detailed overview of the status of
 29 experimental efforts devoted to directional dark matter detection may be found
 30 in [11]. A common issue amongst these detectors is the fact that directional
 31 detection requires track reconstruction of recoiling nuclei down to low energies
 32 (a few keV). This can be achieved with low pressure gaseous detectors [12] and
 33 several gases have been suggested : CF₄, ³He + C₄H₁₀ or CS₂. Ideally, recoiling
 34 tracks should be 3D reconstructed [4] with sense recognition [13, 14].
 35 The MIMAC (MIcro tpc MAtrix of Chambers) collaboration [7] is planning
 36 to build a multi-target detector, composed of a matrix of gaseous micro-TPC

*Corresponding author
 Email address: olivier.bourrion@lpsc.in2p3.fr (O. Bourrion)
 Preprint submitted to Elsevier

37 detectors. A pixelized bulk Micromegas [15] is used in order to perform a 3D re-
38 construction of few mm tracks. It is segmented in 350 μm pixels associated to a
39 dedicated ASIC previously described [16]. Indeed, the coordinates in the anode
40 plane (x and y coordinates) are reconstructed by collecting primary electrons
41 produced in the drift region with an electric field (≤ 1 kV/cm) and amplified in
42 the avalanche region (20 \rightarrow 80 kV/cm). The track of the recoil is thus projected
43 on the anode, providing 2D information. As stated above, 3D track reconstruction
44 is needed for directional detection of dark matter. This is achieved by
45 sampling the anode signal every 25 ns. Knowing the electron drift velocity, in-
46 formation on the third coordinate is retrieved.

47
48 To demonstrate the relevance of the concept, a specific acquisition electronic
49 has been developed in order to equip a prototype detector featuring an anode
50 of 3.36×3.36 cm² where 2×96 strips are monitored with these ASICs. This
51 auto-triggered acquisition electronic uses embedded processing to reduce data
52 transfer to its useful part only, i.e. decoded coordinates of hit tracks and corre-
53 sponding energy measurements. To be fully exploited, an acquisition software
54 with on-line monitoring and track reconstruction has been written.

55
56 This paper is organised as follows : section 2 presents the hardware de-
57 sign, emphasizing on the front end digital interface (FPGA) implemented on
58 the acquisition board. Then the acquisition software and the 3D reconstruc-
59 tion strategy are presented in section 3. Eventually, experimental results are
60 presented in section 4.

61 **2. Hardware design and architecture**

62 *2.1. Overview of the MIMAC acquisition board*

63 As shown on figure 1, the acquisition board is composed of 12 front end
64 ASICs, 6 for each coordinate (X and Y). The data processing was split in 3
65 FPGA, one for each side and one for merging the data. The LVDS serial links
66 are directly connected to the XY FPGA, which de-serializes the ASIC compar-
67 ators data. Then the XY FPGA processes each ASIC position data for
68 suppressing the zeros, decoding the coordinates and assembling them with the
69 data coming from the neighbouring ASICs. At the end of the processing, the
70 data in the first level FPGA are time sorted and placed in a data buffer (called
71 position buffer).

72 The two analogue outputs of each ASIC go through peak detectors in order to
73 find the maximum amplitude of the shaper signals. Each high gain peak de-
74 tector is equipped with a comparator whose threshold is tuned by a DAC. The
75 ADC readout is automatically performed by the XY FPGA for each group of
76 16 strips when some track has been detected and if the amplitude of the signal
77 went above the threshold. As for the position data, the energy data are time
78 sorted and placed in a data buffer.

79 At this stage, for both channels (position and energy), 2 data sources are avail-
80 able: one for the X coordinate and an other for the Y coordinate. The merger

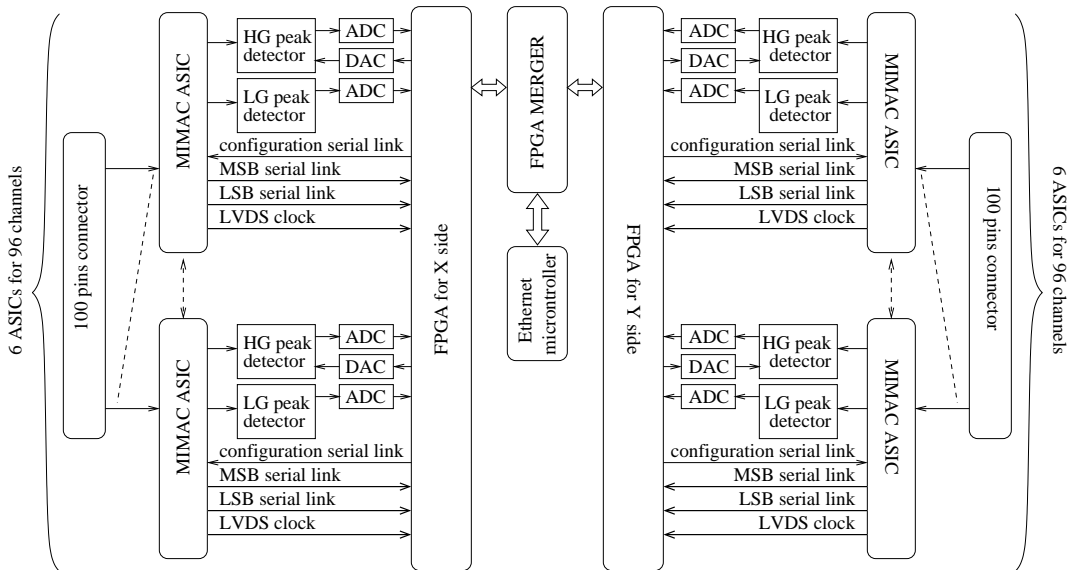


Figure 1: Block diagram of the MIMAC acquisition board

81 FPGA is in charge of concatenating them in a time sorted way and make them
 82 available for data readout. An Ethernet ready micro-controller configured as a
 83 TCP socket server is used as a communication link with the acquisition computer.
 84 It is at the same time used as the slow control interface for:

- 85 • remote configuration of the FPGA (this allows easy upgrades of the firmwares)
- 86 • tuning the energy measurement thresholds
- 87 • tuning the strips discriminators thresholds

88 In the following, we describe the various components of the acquisition board.

89 2.2. Front end ASICs

90 As a preliminary building block for the MIMAC (Micro tpc Matrix of Cham-
 91 bers) framework a front ASIC was developed [16]. These chips were designed to
 92 monitor 16 strips of pixels with low noise charge pre-amplifiers and to provide
 93 in real time their time over threshold.

94 The comparator outputs are coupled to a data serializer with a compression
 95 ratio of 8 in order to reduce consumption and connectivity. Indeed, for the
 96 first phase of the MIMAC project, following this prototype phase, the goal
 97 is to equip an $20\text{ cm} \times 20\text{ cm}$ anode featuring 1024 strips). De-serializing
 98 these data provides a picture of the strips of pixels at a 40 MHz rate. Then,
 99 providing the electron drift velocity in the gas mixture the third coordinate of
 100 the track is reconstructed by using consecutive samples of the strips of pixels.

101 The thresholds are individually tuned by 5 bit current DACs.
 102 For providing a mean to measure the total energy released in the ionisation
 103 channel by the incident particle, the sixteen pre-amplifier outputs are summed
 104 and provided in two gains via two shapers. More details may be found in [16].

105 *2.3. Energy measurement with peak detectors*

106 Each ASIC shaper output is connected to a peak detector (fig. 2) which is
 107 designed to memorise the maximum amplitude when enabled. Both high and
 108 low gain analogical values are digitized by ADCs when the shaper high gain
 109 output goes back below the threshold programmed by a DAC (comparator part
 not shown on fig. 2). The first stage amplifies and inverts the negative input

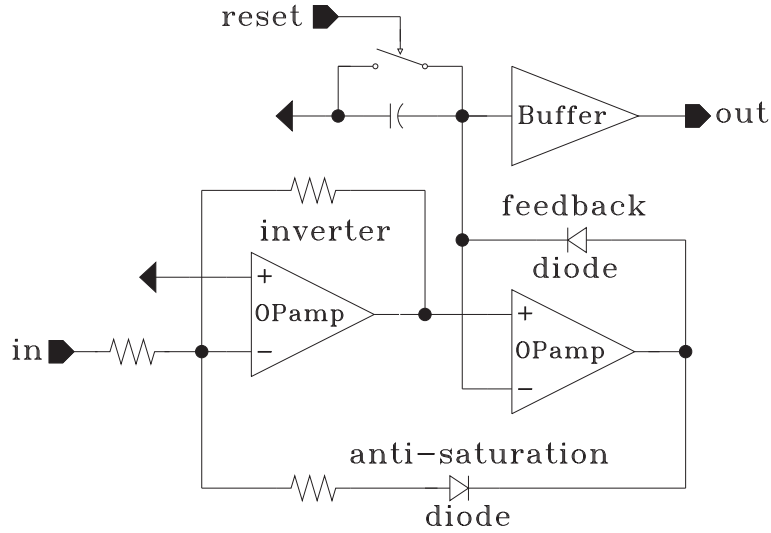


Figure 2: Block diagram of the peak detector used for the energy measurement.

110 signal to deliver a positive signal to the second stage. As long as this signal
 111 increases, the feedback diode stays in conduction mode and the capacitor volt-
 112 age follows the signal. Once the maximum amplitude is reached, i.e. when the
 113 shaper signal starts to decrease, the feedback diode switches in blocking mode
 114 and thus, the peak amplitude is kept in the capacitor. At this stage, the peak
 115 detector amplifier toggles to non linear mode. An anti-saturation loop is imple-
 116 mented in order to maintain the peak detector amplifier differential input to a
 117 minimum value. Indeed one of the bipolar amplifier drawbacks is the fact that
 118 they exhibit a dramatic input leakage current increase when input differential
 119 voltage increases, which would compromise the analogue memorisation func-
 120 tion. The reset signal is used to disable the peak search and also to discharge
 121 the capacitor at the end of the conversion. Bipolar operational amplifiers were
 122 chosen for implementation as it was required to work with low voltage supplies
 123 and thus having rail to rail input amplifiers was mandatory.
 124

125 *2.4. Front end digital interface: XY FPGA*

126 The XY FPGA ¹ is composed of two parts. The first one, identical for each
 127 ASIC, deserializes the data and performs the local triggering, ADC readout and
 128 local data buffering. The second one is in charge of data time sorting and coord-
 129 inate decoding.

130 The deserializer is designed to allow operation with low performance FPGA by
 131 using two shifters working on opposite edges at half of the incoming data fre-
 132 quency (figure 3). The sampling phase is adjusted by setting the DCM (Digital
 133 Clock Manager provided in Xilinx FPGAs) to the appropriate value by slow
 134 control.

The ASIC management is detailed on figure 4. The deserializer first provides

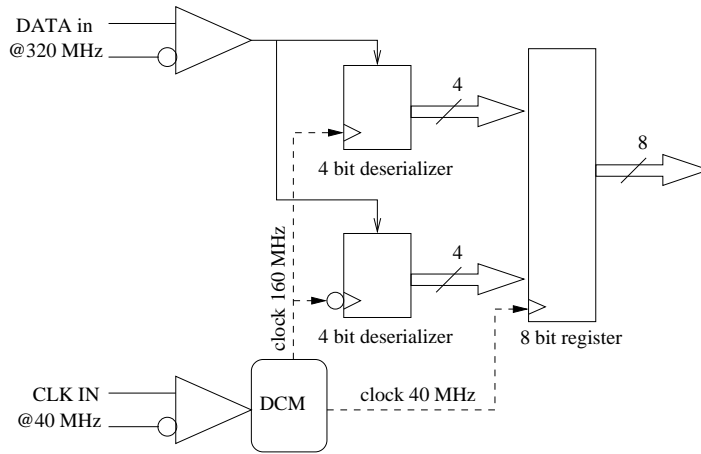


Figure 3: Block diagram of the low cost deserializer

135 data for the local triggering (an OR of the 16 channels), when a trigger is found,
 136 a copy of the free running time counter is inserted in the *raw position memory*,
 137 meanwhile the strip data are delayed by one clock cycle to allow this. After the
 138 time count is written in the memory, the strip data are pushed in the memory
 139 while the stop condition is not fulfilled. Experimental results show that primary
 140 electron distribution can be non continuous and therefore strips can be untrig-
 141 gered for a short amount of time. The stop condition is therefore no trigger on
 142 the monitored channel for more than n clock cycles. This value can be adjusted
 143 by slow control.

145 The memory depth is a key issue. It has to be dimensioned in order to cope
 146 with long tracks like alpha particle, because readout is performed at a much
 147 slower speed than the memory writing. For instance, in ³He at 350 mbar the
 148 drift speed is 16 $\mu\text{m}/\text{ns}$, so an alpha particle arriving orthogonally to the anode

¹so called because the processing is identical on the X and Y side

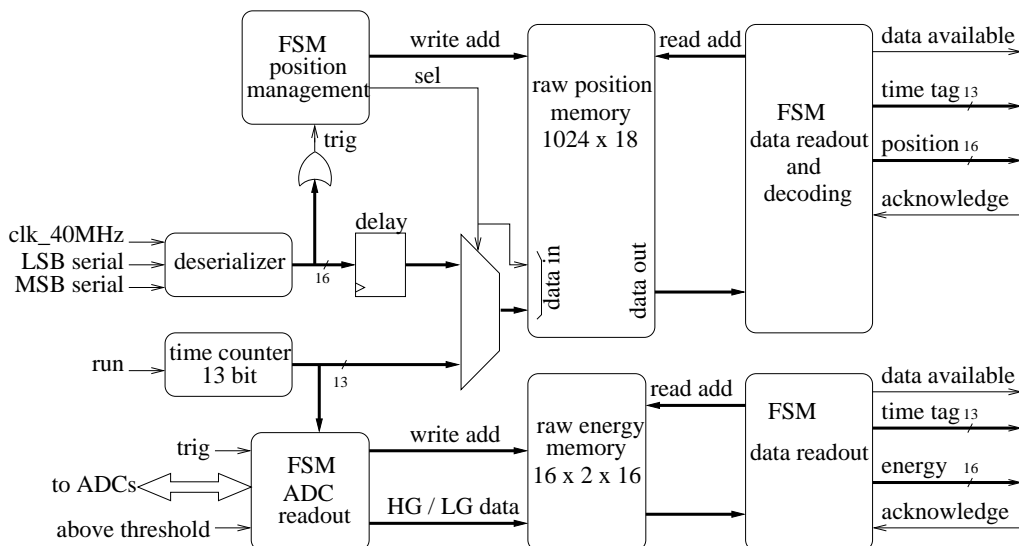


Figure 4: Block diagram of the ASIC management logic

149 will use $\frac{15 \text{ cm}}{16 \mu\text{m/ns}} \times 40 \text{ MHz} \simeq 375$ memory cells. Then, each position word in
 150 memory can potentially be decoded as 16 valid positions. The memory blocks
 151 used in the FPGA are several times larger than this value.

152 The trigger is also used by the energy measurement channel. When detected,
 153 the ADC readout system saves the trigger date and waits until a peak is de-
 154 tected within a predefined time limit (shaping time). If none is detected, a null
 155 value is inserted in the energy memory in order to keep raw position memory
 156 and raw energy memory aligned and facilitate later reconstruction. The raw
 157 energy memory is smaller, because for a full particle track only one amplitude
 158 will be coded in two gains. Distributed RAM is sufficient for this task.

159 Once all data are stored in local buffers, the next step is to assemble them with
 160 the data originating from other ASICs. This operation is done by Finite State
 161 Machine (FSM), like the one used for sorting the position data (figure 5). The
 162 only difference with the one used for sorting the energy data is the position
 163 decoding (*scan word* state), each bit at one in position word is decoded as a
 164 strip number. Starting from the *idle* state, the FSM waits for the first ASIC
 165 (or group) to present data. When it is the case, the current date is saved and
 166 the position decoding is performed. Then the FSM looks if an other group
 167 presents position data marked with the same date, if yes the data are decoded
 168 and appended to the output buffer in the same time slot, if not the time slot is
 169 closed and the search for a new time slot continues. At this stage, 2 possibilities
 170 remain:

- 171 • no more data are available and the FSM returns to *IDLE*

172 • data are still available and the earliest data has to be found

173 For that, a scan of the dates is made (*seek_next_group*) in order to find the
 174 first ASIC in time. This scanning is complexified by the fact that the time
 175 counter has a short span (13 bit which corresponds to ~ 1.31 ms), therefore it is
 176 performed in 2 stages. First the search is performed from the current date up
 177 to the maximum counter value, and if not successful, the current date is set to
 178 zero and the searching is performed again until the group is found (*check roll*
 179 *over* state).

180 Position data and energy data are stored in separate buffers (see template in
 181 table 1). Both tables are organised in order to optimize bit usage and therefore
 182 data are encoded on 16 bit. For a specific time-stamp, all useful position or
 183 energy data are grouped under a unique TAG. The time slice is closed by the
 184 *End of TAG* label.

bit	15	14	13	12	11	10	9	8	7	6	5	4	3	2	1	0
TAG	0	date														
position DATA n	1	0									ASIC #		strip #			
energy DATA n	1	0	ASIC #				ADC value									
End of TAG	1	1	unused													

Table 1: Organisation of the 16 bit words containing position or energy information.

185 2.5. FPGA merger

186 This FPGA is in charge of merging the data from the X and Y side. For
 187 this task, it is working similarly to the sorting FSM of the XY FPGA, the only
 188 difference being the fact that only 2 data producers are managed instead of
 189 6. Once the data are processed, they are stored in large buffers. They can be
 190 accessed directly for readout by the Ethernet micro-controller. Also, being the
 191 direct interface with the micro-controller, it is used as the slow control interface
 192 for:

- 193 • Enabling or disabling an ASIC
- 194 • Activating the calibration mode. In this mode a constant pattern is sent
 195 by the ASICs and for reducing the data amount, only one out of 65536
 196 triggers is accepted.
- 197 • Configuring the energy channel thresholds

198 2.6. Ethernet interface

199 This interface is based on a 32 bit micro controller, using a flash memory
 200 and 16 MB of SDRAM. Its purpose is to provide an easy computer interface
 201 and to test the possibility for multi chamber acquisition.

202 At power up, a TCP socket server service is started and the acquisition computer
203 (the client) can open a socket and communicate with the hardware via a custom
204 protocol. It is used for slow control and acquisition, they are implemented in 2
205 threads. When in run mode, the acquisition thread is resumed and start polling
206 the empty flags of the position and energy buffers, once a non empty flag is
207 found, the corresponding fifo level is read. Then the appropriate number of
208 readout is made and the data are transmitted through the socket with a header
209 specifying the data type and count.

210 In order to allow flexibility and easy prototyping, the micro-controller firmware
211 is the only one resident on the electronic board and the 3 FPGA are remotely
212 reconfigured at each start up via the TCP socket.

213 **3. Acquisition software**

214 The acquisition software was developed in C++ and coded to allow operation
215 on Linux and Windows platforms. In order to keep a good separation between
216 functionalities, it is built with three different parts as described below.

217 *3.1. Software driver*

218 The low level driver is in charge of providing low level functions for con-
219 trolling the hardware and managing the acquisition. It features a platform
220 independent non blocking socket client manager, routine for reading FPGA
221 configuration file and remotely configuring them, methods for interpreting po-
222 sition and energy threshold files and set DAC values.

223 For a proper tuning of the serializers sampling phase, a scanning algorithm is
224 also provided. Basically, it puts the hardware in calibration mode (in order
225 to significantly decrease the trigger rate), validate one ASIC at a time and try
226 every possible value of de-phasing (256 values) and record the results of the
227 reception of a known test pattern. The test pattern is supposed to be received
228 correctly many thousand times in order to consider that the sampling phase
229 is correct for the selected ASIC. When the stability range common to the 12
230 ASICs has been determined, the mean value is computed and transferred to the
231 XY FPGA.

232 The data acquisition has to be performed with a blocking call method (returns
233 only when the required number of bytes are read or when a time out occurs).
234 This function reads data frame received from the socket and separates them be-
235 tween energy and position. They are then pushed in 2 STL (Standard Template
236 Library) queues. The readout is performed this way, because the electronic pro-
237 cessing time from particle interaction to data available in computer varies with
238 energy and position data path.

239 *3.2. Acquisition thread and event building*

240 The acquisition is performed in a thread loop, with the software driver and
241 Qt framework [17]. The algorithm of the event building is depicted on figure
242 6. When the thread is awoken, it starts looping on the data readout method

243 provided by the software driver. As soon as both position and energy queues
244 are not empty any more the event building processing part starts.

245 In order to properly assemble an event, the position queue is processed first in
246 order to find out when it starts and when it stops. All triggered strips with
247 dates separated by less then the allowed number of empty clock ticks are kept
248 as member of the same event. But as soon as the date of the currently processed
249 triggered strips jumps from more than the allowed number of clock ticks, it is
250 considered to be a member of the next event and the current event position
251 retrieval is finished. At this stage the event start date and duration are known
252 and the corresponding energy data may be found in the energy queue. In other
253 word, the continuous triggering of the anode defines an event.

254

255 *3.3. Individual strip threshold calibration*

256 In order to operate correctly a MIMAC prototype equipped with the ASIC
257 described, each strip threshold has to be properly tuned. This task would be
258 cumbersome if not automated, especially when the aim is to monitor 1024 strips
259 per chamber. Therefore an automated calibration method was developed and
260 tested with the prototype.

261 The procedure is to shut down all high voltage applied to the chamber in order
262 to have no real events and to try to find the best DAC setting that will put the
263 thresholds just above noise. This is done by running short acquisitions (~ 15 s)
264 with each settings until the good one is found.

265 First the calibration algorithm will start with all thresholds set at their maxi-
266 mum values and try to decrease them as long as each individual strip doesn't
267 trigger (all strip thresholds are tuned at the same time). When a strip has
268 reached its lowest threshold, it is marked as such. But since there is some
269 crosstalk on the board, a second phase is necessary. It has been observed that,
270 when other thresholds lower, some noise is generated on the acquisition board
271 and picked again by the strips whose threshold were marked as tuned. So in the
272 second step, the threshold is increased, one digit at a time, until the triggering
273 is stopped. The chamber is declared calibrated when all strip thresholds are
274 marked as having reached their minimum value and no more trigger is counted
275 in the acquisition.

276 *3.4. Graphical interface and event display*

277 As stated above, the readout is performed in 2D with strips of pixels, which
278 means that an event is considered as valid if, for a given time slot, at least one
279 strip of pixels in each dimension (X and Y) is fired. When such a coincidence
280 happens, the position of the fired pixels can be evaluated as the intersection of
281 the fired X strips and Y strips. Each time slot gives access to a 2D slice of the
282 track, and each slice following each other will lead to a 3D track.

283 Once an event is built by the 3D reconstruction algorithm, it has to be
284 displayed with a visualization software both in online and offline modes. This
285 real-time visualisation software allows to monitor several parameters of the de-
286 tector during a run, such as the energy deposit, the position of the interaction

287 and the length of the track. Real-time access to these information offers the
288 possibility to adjust the detector parameters, such as the gas pressure, anode
289 and micro-mesh voltages or the electronic thresholds in order to reach optimized
290 working conditions during an acquisition run. Furthermore, the event display
291 software enables the testing and debugging of the reconstruction software and
292 the analysis strategy in an offline mode.

293 To meet these specifications, a visualization tool mainly based on the Qt [17]
294 and ROOT [18] framework was developed. Qt offers a well documented user
295 interface framework implemented in C++. A third interface layer named “Qt
296 layer” [19] was used to build the application software.

297 The user interface of the online software is segmented in several tabs:

- 298 • one dedicated only to acquisition process: automated calibration, start/stop
299 runs
- 300 • another tab displays the energy spectrum (both in low and high gain) in
301 real time
- 302 • Event display, used also in offline mode, provides projection of the 3D
303 track

304 As shown on figure 7, the main canvas of the event display panel is segmented
305 in 4 panels:

- 306 • the top left panel represents a 2D view of the event, as seen by the anode
307 (XY projection)
- 308 • the top right panel shows the evolution of the number of fired strips versus
309 time, for the X side (solid line curve) and the Y side (dashed line curve)
- 310 • the bottom pads represent projections of the track on the XZ plane (left
311 panel) and YZ plane (right panel)

312 Event by event display of the projected 3D track (XY, XZ and YZ his-
313 tograms) is provided by the visualisation software. Whether in online or offline
314 mode, the list of event to display can be adjusted through several criterion like:
315 number of images (equivalent to length along Z axis), energy deposit or even a
316 combination of those.

317 4. Experimental results of the MIMAC Data AcQuisition

318 As required by the specifications, the MIMAC DAQ is able to reconstruct
319 3D tracks of nuclear recoils and electrons between a few keV and hundreds of
320 keV.

321 First experimental results were obtained with a 5.9 keV X-ray source (^{55}Fe)
322 producing 5.9 keV electrons in a 350 mbar $^4\text{He} + 5\% \text{C}_4\text{H}_{10}$ mixture used as
323 detection medium. These electron tracks (figure 9) have a specific length over
324 energy ratio and will be typical background events in the final MIMAC dectector
325 designed to detect dark matter in an underground laboratory.

326 Ultimately, the goal of MIMAC is to reconstruct recoil tracks of nuclei in
327 3D. In order to test the MIMAC prototype associated to the dedicated ac-
328 quisition electronics with nuclei recoils, the detector was placed in front of a
329 mono-energetic neutron beam at the Amande facility [20]. Depending on the
330 target gas used, recoils of hydrogen ions, helium ions or event fluorine ions were
331 reconstructed [21].

332 For instance, on figure 8, a 100 keV proton recoil obtained in a 350 mbar
333 $^4\text{He} + 5\% \text{C}_4\text{H}_{10}$ mixture is displayed in three dimensions. Left panel presents
334 the raw 3D track, ie images of the anode in each z slice. Right panel presents
335 the barycentre of each z slice. This shows the possibility to achieve 3D track
336 reconstruction of recoiling nuclei in low pressure gaseous TPC. Figure 9 presents
337 the same views of 5.9 keV electrons, highlighting the possibility to reach low
338 energies with this technique. This last event is of crucial interest as it features a
339 typical background event for Dark Matter search. A comprehensive study of an-
340 gular resolutions obtained with this 3D reconstruction method will be presented
341 in a forthcoming paper [22]. This dedicated acquisition electronics associated
342 with 3D reconstruction software offers a major breakthrough towards 3D recon-
343 struction of low energy tracks, thus opening great opportunities for directional
344 Dark Matter search [21].

345 5. Conclusion

346 A dedicated acquisition electronics with auto triggering feature and a real
347 time track reconstruction software have been developed within the framework
348 of the MIMAC project of detector. It has been shown by experimental results,
349 that the MIMAC ASIC [16], the prototype acquisition board (fig. 10) and soft-
350 ware coupled together offer great possibilities for 3D track reconstruction and
351 ultimately for directional dark matter detection.

352

353 Acknowledgement

354 C.G. and the MIMAC collaboration acknowledge the ANR-07-BLAN-0255-
355 03 funding.

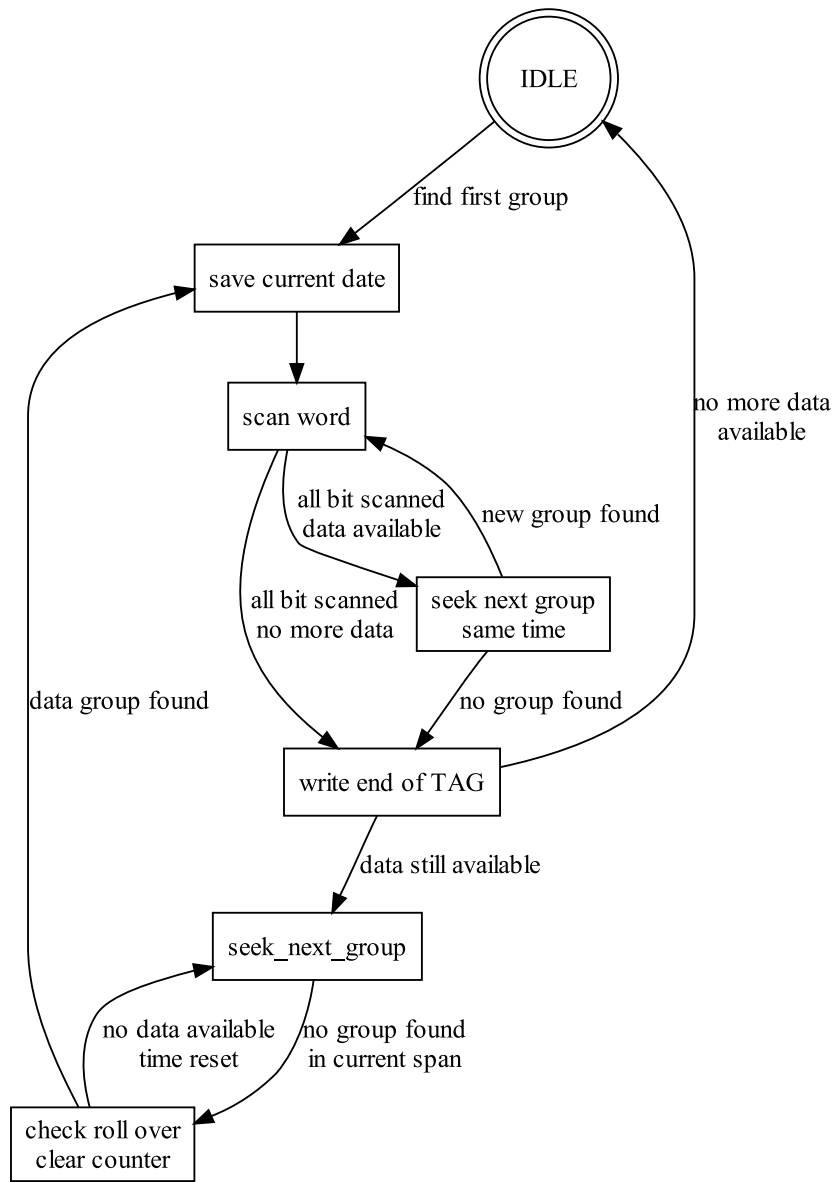


Figure 5: Description of the finite state machine (FSM) used for position data sorting

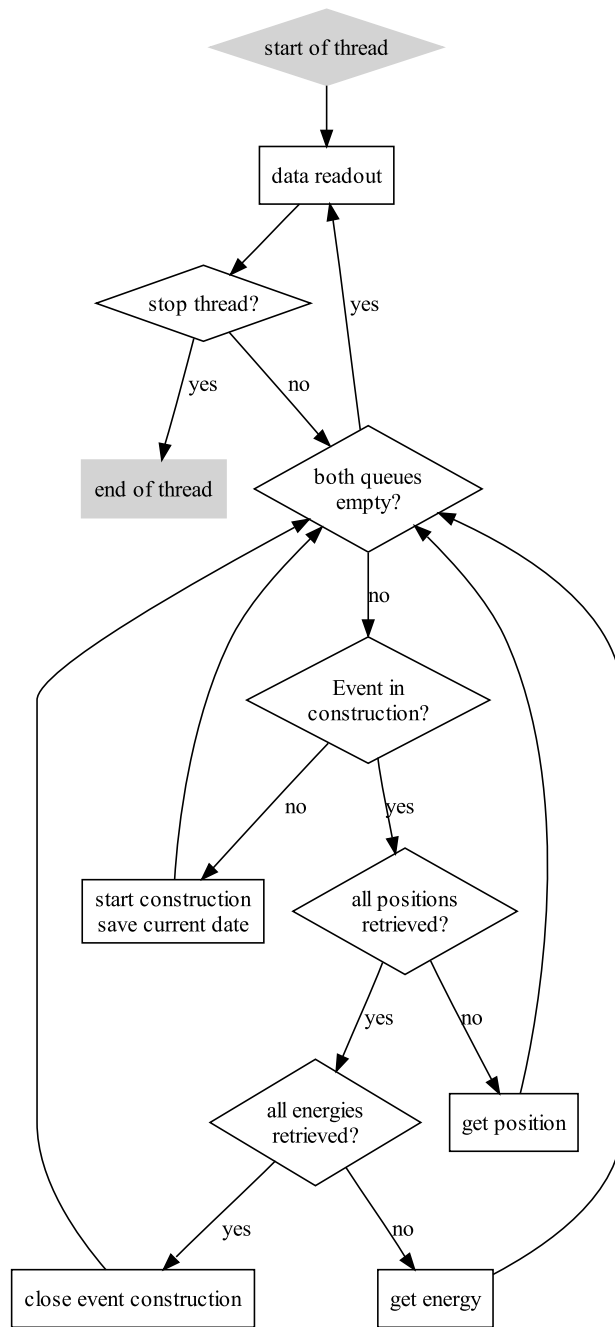


Figure 6: Event building algorithm embedded in the acquisition thread

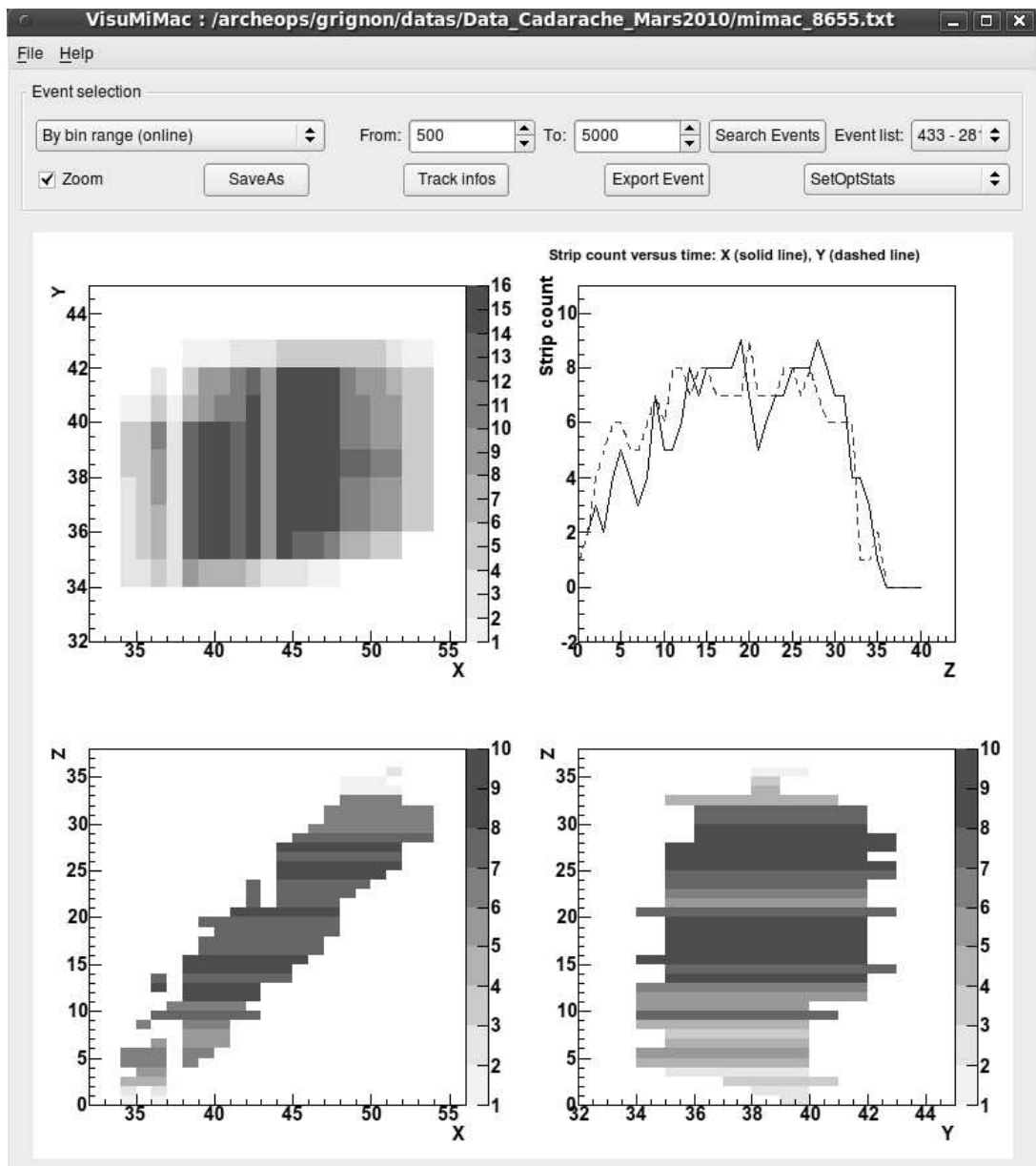


Figure 7: Snapshot of the event display tab of the MIMAC real-time visualization software. Top left panel represents a 2D view of the event, as seen by the anode (XY projection). Top right panel shows the evolution of the number of fired strips versus time, for the X side (solid line curve) and the Y side (dashed line curve). Bottom pads represent projections of the track on the XZ plane (left panel) and YZ plane (right panel)

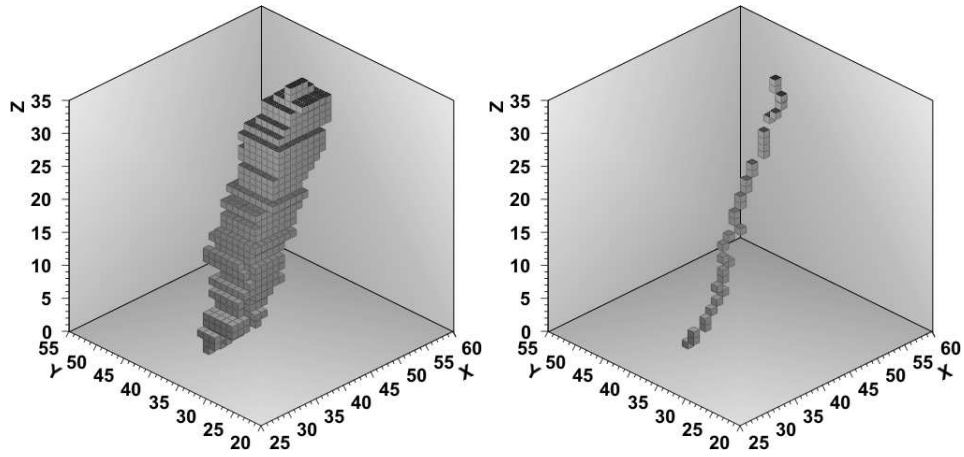


Figure 8: 100 keV H recoil in a 350 mbar $^4\text{He} + 5\% \text{C}_4\text{H}_{10}$ mixture: left panel represents the raw 3D track while the right panel shows barycentres of each time slice

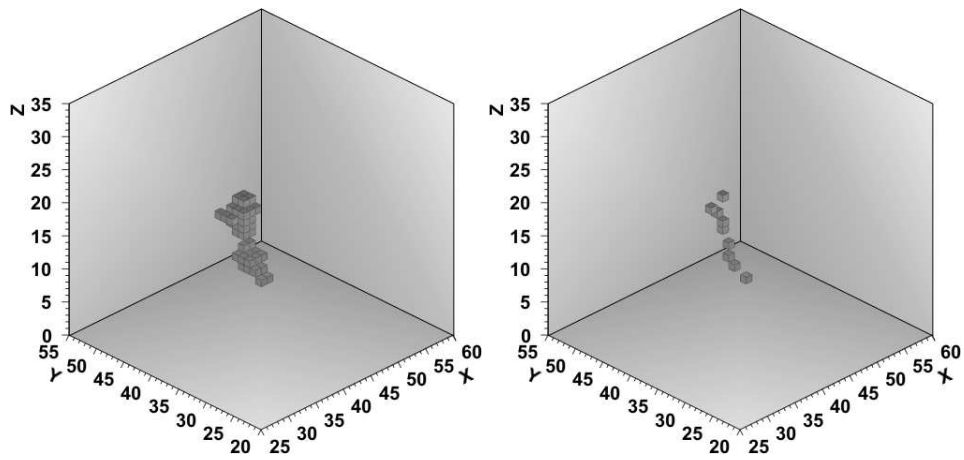


Figure 9: 5.9 keV electron recoil in a 350 mbar $^4\text{He} + 5\% \text{C}_4\text{H}_{10}$ mixture (barycentre on the right panel)

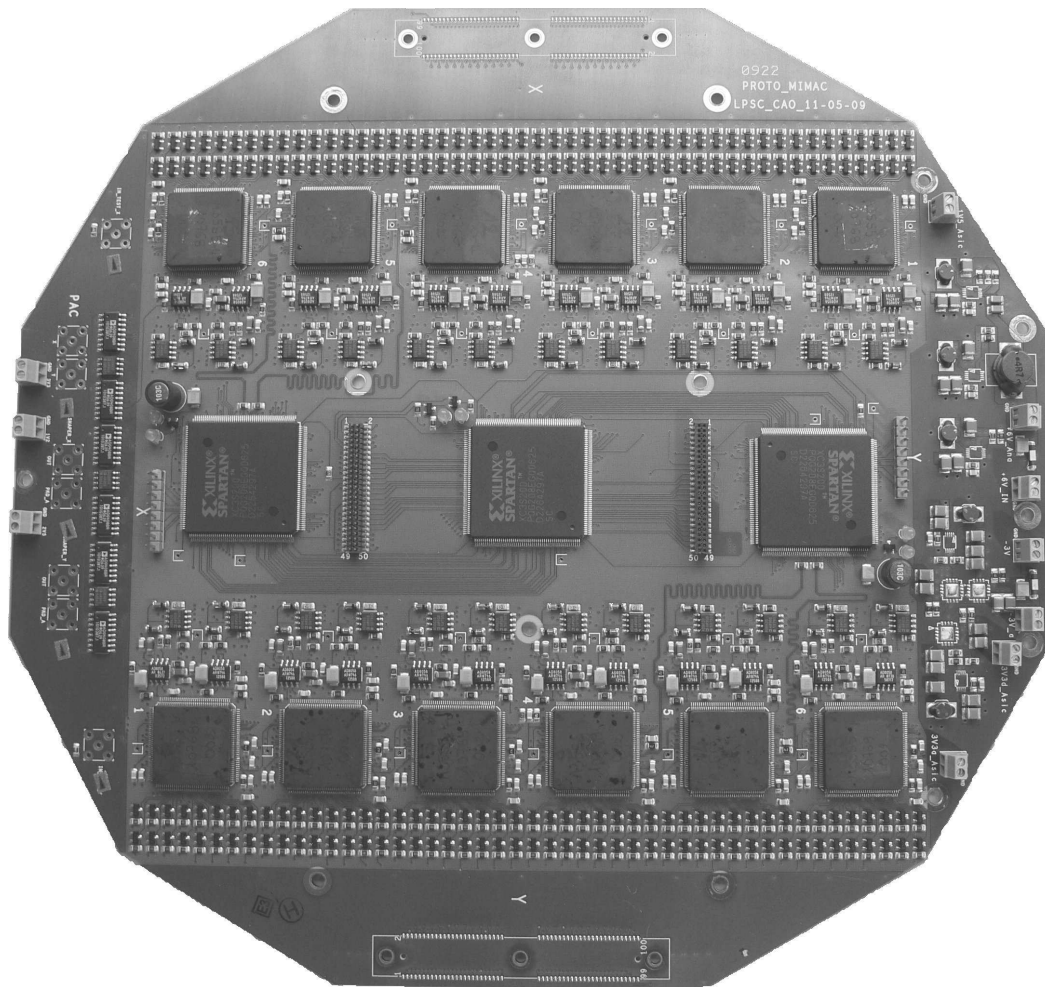


Figure 10: Picture of the 260 mm \times 246 mm MIMAC acquisition board. Ethernet interface board and connectors are missing on this view. X side of the detector is connected on the top connector and Y side on the bottom one. The 2 \times 6 ASIC are fed by the connectors. In the middle the 3 FPGA perform the processing.

356 **References**

- 357 [1] D. N. Spergel, Phys. Rev. D **37** (1988) 1353
- 358 [2] B. Morgan, A. M. Green and N. J. C. Spooner, Phys. Rev. D **71** (2005)
359 103507
- 360 [3] B. Morgan and A. M. Green, Phys. Rev. D **72** (2005) 123501
- 361 [4] A. M. Green and B. Morgan, Astropart. Phys. **27** (2007) 142
- 362 [5] A. M. Green and B. Morgan, Phys. Rev. D **77** (2008) 027303
- 363 [6] J. Billard *et al.*, arXiv:0911.4086
- 364 [7] D. Santos *et al.*, J. Phys. Conf. Ser. **65** (2007) 012012
- 365 [8] G. J. Alner *et al.*, Nucl. Instr. Meth. A **555** (2005) 173.
- 366 [9] K. Miuchi *et al.*, Phys. Lett. B **654** (2007) 58
- 367 [10] G. Sciolla *et al.*, J. Phys. Conf. Ser. **179** (2009) 012009
- 368 [11] S. Ahlen *et al.*, Int. J. Mod. Phys. A **25** (2010) 1
- 369 [12] G. Sciolla and C. J. Martoff, *New J. Phys.* **11**, 105018 (2009)
- 370 [13] D. Dujmic *et al.*, Nucl. Instrum. Meth. A **584** (2008) 327
- 371 [14] S. Burgos *et al.*, arXiv:0809.1831
- 372 [15] Y. Giomataris *et al.*, Nucl. Instr. and Meth. **A560** (2006) 405
- 373 [16] J. P. Richer *et al.*, arXiv:0912.0186, to appear in Nucl. Instr. Meth. A,
374 doi:10.1016/j.nima.2010.04.041
- 375 [17] Qt framework, <http://qt.nokia.com/>
- 376 [18] ROOT, an object-oriented data analysis framework.
377 <http://root.cern.ch/>
- 378 [19] V. Fine, Nucl. Instr. and Meth. **A502** (2003) 681-683,
379 <http://root.bnl.gov/>
- 380 [20] A. Allaoua *et al.*, Radiat. Meas. **44** (2009) 755-758
- 381 [21] D. Santos *et al.*, in preparation
- 382 [22] C. Grignon *et al.*, in preparation